Materials Chemistry and Physics 266 (2021) 124573

Contents lists available at ScienceDirect

Materials Chemistry and Physics

journal homepage: www.elsevier.com/locate/matchemphys

Assessment of biocompatibility of novel TiTaHf-based high entropy alloys for utility in orthopedic implants

S. Gurel [a,1], A. Nazarahari [a,1], D. Canadinc [a,*], H. Cabuk [b], B. Bal [c]

[a] Koc University, Advanced Materials Group (AMG), Department of Mechanical Engineering, Istanbul, 34450, Turkey
[b] Istinye University, Department of Orthopedics and Traumatology, Istanbul, 34517, Turkey
[c] Abdullah Gül University, Department of Mechanical Engineering, Kayseri, 38080, Turkey

HIGHLIGHTS

- Novel TiTaHf-based high entropy alloys were immersed in fetal bovine serum.
- Hydroxy apatite and passive oxide layer formation was observed upon immersion.
- TiTaHfNb alloy shows a high potential for utility in knee implants.

ARTICLE INFO

Keywords:
High entropy alloy
Biocompatibility
TiTaHfNbZr
TiTaHfMoZr
TiTaHfNb

ABSTRACT

This paper presents the findings of experimentally observed corrosion response of novel TiTaHf-based high entropy alloys (HEAs) in fetal bovine serum (FBS) to evaluate their biocompatibility in presence of proteins and potential to be used as implant materials. Particularly, TiTaHfNb, TiTaHfNbZr and TiTaHfMoZr HEAs were subjected to static immersion experiments in FBS media, and both the HEA samples and the immersion fluids underwent thorough characterization. The findings presented herein show that Zr and Mo addition to the TiTaHf solid solution increased the total ion release from the resulting HEAs in FBS, while the TiTaHfNb HEA became prominent in terms of biocompatibility owing to the reduced ion release in FBS. Moreover, hydroxy apatite (HA) formation was evident on the surfaces of all three HEAs upon immersion in FBS, indicating the potential of the three TiTaHf-based HEAs to form desired binding with the human bone. Considering the fact that passive oxide layer formation facilitating lower susceptibility to corrosion in long-term applications was also observed in the studied HEAs, further elaboration on their mechanical and biological responses is warranted for the sake of a comprehensive assessment regarding their utility as orthopedic implant materials.

1. Introduction

Apart from the delicate geometrical design, medical implants need meticulous material selection in order to function properly in their specific roles, including various applications such as total hip prostheses, bone fixation plates and dental implants. Such applications demand combination of high corrosion resistance, toughness and wear resistance. Stainless steel was the earliest material which could fulfill these requirements all at once to a certain extent, and even though it has been replaced by CoCr or Ti alloys in many applications within the recent years, it is still a popular metallic biomaterial for bone replacements, fixations or joint prostheses [1]. However, it has been shown that this alloy is responsible for development of allergic symptoms such as rash and blister patches, which have been associated mainly with nickel ion release [2,3]. Therefore, despite its high strength and good corrosion resistance, toxic ion release from stainless steel into the human body warranted the search for alternative metallic implant materials.

The most well-known outcomes of these efforts are alloys of titanium, such as Ti6Al4V and NiTi. In these alloys, the titanium-oxide layer provides a remarkable corrosion resistance, as well as better biocompatibility, which is due to the osseointegration process between the implant and the bone [1,4–8]. However, toxic ion release (Al, V from Ti6Al4V and Ni from NiTi) is an issue with these alloys, resulting in biocompatibility deterioration which can cause unfavorable

* Corresponding author.
E-mail address: dcanadinc@ku.edu.tr (D. Canadinc).
[1] S. Gurel and A. Nazarahari equally contributed to this work.

https://doi.org/10.1016/j.matchemphys.2021.124573
Received 31 July 2020; Received in revised form 3 January 2021; Accepted 30 March 2021
Available online 3 April 2021

physiological effects, such as allergic reactions, decreased fertility or even damage to the nervous system [9,10]. Moreover, The ion release can cause weak interfacial bond between the alloy and the bone, adversely affecting the implant's osseointegration [11]. Another disadvantage of these alloys is the mechanical property mismatch with the human bone, which can significantly alter the functionality of the implant in the long term. In particular, mismatch of stiffness results in stress shielding effect that damages the bone tissue, and eventually causes wear-induced osteolysis owing to material detachment from the metal implant [4,12]. Therefore the search for alternative materials satisfying both biocompatibility and mechanical properties for replacing bone tissue has gained momentum in the recent years [13–16]. In addition, the durability of an orthopedic implant depends on both biocompatibility of the implant and its tribological performance, where the latter involves stiffness, scratch resistance and surface roughness [17]. For instance, during the last few decades CoCr alloys have become the mostly utilized material for surface arthroplasties, however; owing to surface wear and osteolysis, revision rates for arthroplasties could reach up to 50% in the 15 year follow up [18]. In order to decrease this rate, different materials such as ceramics and Ti-based alloys have been employed but the revision rates have remained still considerably high [19]. Apparently, the need for implant materials with a high surface abrasion resistance and good osteointegration still exists.

An alternative class of materials emerged as a consequence of recent efforts to manufacture high toughness alloys for aerospace industry, namely the high entropy alloys (HEAs), which have also opened a new window for designing metallic alloys for different applications due to their exceptional properties. The HEAs usually consist of at least four alloying elements with equimolar or close to equimolar percentages, in other words, the HEAs are multi-principle element alloys. This generates high configurational entropy, leading to a very stable single phase formation, which eventually brings about excellent corrosion resistance, high fracture toughness, high strength and hardness [20–23]. Recently, numerous studies have been conducted to discover potential applications of HEAs, especially in the biomedical field. In most scenarios, HEAs composed of nontoxic transition elements, such as Ti, Hf, Nb and Mo, are subjected to biocompatibility experiments that involve immersion of the HEA samples into solutions simulating body fluids, followed by the assessment of changes both within the metal and the fluids [15,20,24,25]. So far, a limited number of studies have explored the effects of different corrosive media on the biocompatibility of HEAs, where Ringer's solution, phosphate-buffered saline (PBS), simulated body fluid (SBF) and artificial saliva (AS) were considered as the corrosive media acting on bulk $(TiZrNbTa)_{90}Mo_{10}$, TiTaHfNb, TiTaHfNbZr, TiTaHfMoZr and $Ti_{1.5}ZrTa_{0.5}Hf_{0.5}Nb_{0.5}$ HEAs [13–16,25,26]. Based on the superior corrosion resistance of these materials demonstrated in the aforementioned studies, some of them, including the TiTaHfNbZr alloy, were also successfully used to coat conventional biomedical alloys, such as NiTi and Ti6Al4V, in order to enhance their biocompatibility, such that the passive oxide layer forming on the surface further enhanced the corrosion resistance by restricting the ion release from the substrate alloys [27–29].

Generally, chloride ion concentration or pH of the media play a crucial role in the formation and properties of the passive layer forming on conventional implant alloys [30]. However, a comparison of an in-vitro sample of a CoCrMo implant with a collected in-vivo sample revealed that the proteins in human body also clearly have an influence on this passive layer, as evidenced by the tarnished film that formed on the surface of the in-vivo sample [31]. In a later study supporting this argument, where the effect of addition of albumin and fibrinogen to PBS on pure Co and Cu, and cast CoCrMo alloy was studied, the proteins were shown to enhance the corrosion of Co and Cu while they inhibited corrosion of Mo, demonstrating that the corrosion behavior depends on the interaction of proteins with the specific metallic elements [32]. For instance, it has been shown for AISI 304 and AISI 316L stainless steels that the proteins of albumin, g-globulin, fibrinogen and transferrin can behave similar to complex agents, hindering the formation of a passive layer, eventually leading to pronounced ion release [33]. These findings warrant the need for including organic corrosive media in the biocompatibility and corrosion testing of potential biomedical alloys in order to properly simulate the actual human body conditions while assessing their potential utility as implant materials.

Fetal bovine serum (FBS) can be a plausible choice for such corrosive medium exhibiting the aforementioned characteristics. This serum has been used in biological studies for decades as a generic supplement for cell growth due to existence of broad range of proteins it contains, which provides a similar condition to the human body while healing after implantation surgery [34,35]. Therefore, several studies have been conducted using FBS to culture cells on the surface of the conventional implant alloys to assess the interaction of living cells with the alloys and their corresponding proliferation, as well as the corrosion response of the alloys [36–39]. This method of study is a great tool to evaluate the biocompatibility of the alloys, but one shortage of the previous works is that media was in contact with the alloy for a relatively short time. This can be an issue since the passive layer properties have been shown to change with time due to dissolution-reformation cycles [40]. For instance, significant differences between the passive oxide layer characteristics of NiTi samples immersed in PBS for short time periods and those immersed in FBS for longer periods were reported, laying out the effects of both protein-surface interactions and the duration of contact between the alloy and the corrosive media [41]. Currently, such an assessment of the reaction of TiTaHf-based HEAs to FBS for considerable immersion periods is missing to the best of the authors' knowledge, which constitutes one of the major motivations for carrying out the study presented herein.

In order to accomplish the aforementioned task, three TiTaHf-based HEAs, namely the TiTaHfNb, TiTaHfNbZr and TiTaHfMoZr alloys, were investigated in this study. Specifically, in a recent series of studies the authors have demonstrated the potential of these HEAs to be utilized in orthopedic and orthodontic implants in both bulk form and as coating material, where the biocompatibility was assessed from different points of view, including static biocompatibility and tribological performances [15,16,27–29]. In order to complete the biocompatibility assessment of these alloys by accounting for the protein-metal interactions, which is very crucial especially for orthopedic implantation processes, such as total knee arthroplasty (TKA) [42,43], static immersion experiments were carried out on all three HEAs in FBS in the current work. The findings show that both protective passive oxide layer and bone-like appetite formation was evident on the sample surfaces, further supporting the previously claimed biocompatibility of these alloys. The results also warrant conduction of cell culture studies on these TiTaHf-based HEAs in order to further assess their suitability to be utilized as orthodontic implant materials.

2. Materials and methods

Three different high entropy alloy disks with a 50.1 mm diameter and 6.1 mm thickness were produced using vacuum arc melting (VAR) and 99.9% purity elements resulting in the compositions shown in Table 1. These disks were cut by wire electrical discharge machining (EDM) in form of 10 mm × 5 mm × 1 mm bulk samples. 12 Samples (4 from each HEA disk) were mechanically grinded under running water using emery papers with grit size ranging from 120 to 2500. Grinding was carried out with caution to only remove a layer of negligible

Table 1
Chemical compositions of the studied HEAs in atomic %.

Material	Ti	Ta	Hf	Nb	Zr	Mo
TiTaHfNb	50	16.7	16.7	16.7	0	0
TiTaHfNbZr	20	20	20	20	20	0
TiTaHfMoZr	20	20	20	0	20	20

thickness from each samples' surface, including the oxides and contamination. Subsequently, polishing the samples was done using 0.3 μm alumina slurry until mirror-like surface appearance was obtained. In order to remove any contaminants introduced by the sample preparation process, samples were cleaned by immersing in de-ionized water and then ethanol bath inside an ultrasonic cleaner for 5-min intervals.

Prior to static immersion tests, mass of each dry sample was measured using a scientific scale (Precisa XB 220A) and then the samples were immersed in fetal bovine serum (FBS, Biosera FB-1101) inside 50 ml polypropylene tubes. The necessary amount of serum was calculated according to a volume-to-surface area ratio of 10 ml/cm^2. In order to simulate human body temperature and its effect on corrosion, tubes were positioned inside an electronically controlled water bath at a constant temperature of 37 °C. Subsequently, samples were collected following 1, 7, 14 and 28 days of immersion. After collecting the samples from the tubes, they were washed with de-ionized water, dried using air blow, and their masses were measured.

In order to investigate the microstructures of and uncover the phases present in the samples, X-ray Diffraction (XRD) technique was used on a Bruker D2 Advanced X-ray diffractometer. The Cu-Kα source operating at 30 kV and 10 mA was used with the constant incident angle of 5° while the acquisition angle changed over the 5°–90° range with a 0.02° increment. A scanning electron microscope (SEM, FEI – Quanta 200 FEG) was employed to investigate the surface morphology of the samples, and it was equipped with an energy-dispersive X-ray spectroscopy (EDX) detector. In order to measure the quantity of metallic ions released into the FBS during immersion tests, the solution remaining from each static immersion experiment was analyzed employing an inductively coupled plasma - mass spectrometer (ICP-MS, Agilent 7700x) and compared with the blank FBS sample. X-ray photoelectron spectroscopy (XPS, Thermoscientic, Al K-α radiation) was used to investigate surface properties of the samples and detect the elements present on the sample surfaces, which were subjected to ion etching to establish the XPS depth profiles.

3. Results and discussion

The XRD patterns of TiTaHfNb, TiTaHfNbZr and TiTaHfMoZr before the immersion tests are shown in Fig. 1, where the peak values and lattice parameters were calculated utilizing Bragg's Law [20,44,45]. The XRD results illustrate the BCC-structured solid solution of TiTaHfNb, TiTaHfNbZr and TiTaHfMoZr with the lattice parameters determined as 3.329 Å, 3.340 Å, and 3.362 Å, respectively. Although only a few studies on these three HEAs have been forwarded to date, the XRD results are consistent with the previously reported results in the literature [16,25,46,47].

Fig. 2 shows the total ion concentration of FBS for each sample following the immersion tests for 1, 7, 14 and 28 days. While the total ion concentration in FBS increased continuously within the first two weeks upon immersion of the TiTaHfMoZr HEA in it, it remained nearly constant for the following two weeks, bringing the total ion concentration to a level similar to those measured in FBS samples upon immersing the TiTaHfNb and TiTaHfNbZr HEAs in it. Moreover, the ICP-MS results obtained from FBS samples in which the TiTaHfNb, TiTaHfNbZr and TiTaHfMoZr HEAs were immersed revealed that the amount of Ti release is significantly higher as compared to the other constituents (Ta, Hf, Nb, Zr and Mo) following a 28-day immersion period (Table 2 and Fig. 3). Especially the significant amount of Ti ion release from all three HEAs within the first 7 days of immersion is a strong indication of the initial dissolution of Ti-oxide layer on the samples, considering the fact that all three HEAs have been proven to form a stable solid solution and form a protective Ti-oxide layer on the surface upon immersion in corrosive media [15]. On the other hand, the TiTaHfMoZr HEA released the least amount of Ti as compared to the TiTaHfNb and TiTaHfNbZr HEAs, however; high amount of Mo release from the TiTaHfMoZr HEA was observed during the immersion tests (Table 2 and Fig. 4). Indeed, Mo addition into TiTaHf-alloy led to a high amount of Mo ion release (Table 2 and Fig. 4), exceeding the amount of Nb ion release from TiTaHfNb and TiTaHfNbZr into the FBS, indicating that replacement of Nb with Mo might significantly alter the stability of the TiTaHf-based HEAs. In particular, the addition of Mo into TiTaHf-based alloy gives way to a non-homogeneous elemental distribution during the manufacturing process due to the long "hands-on" time [48], such that

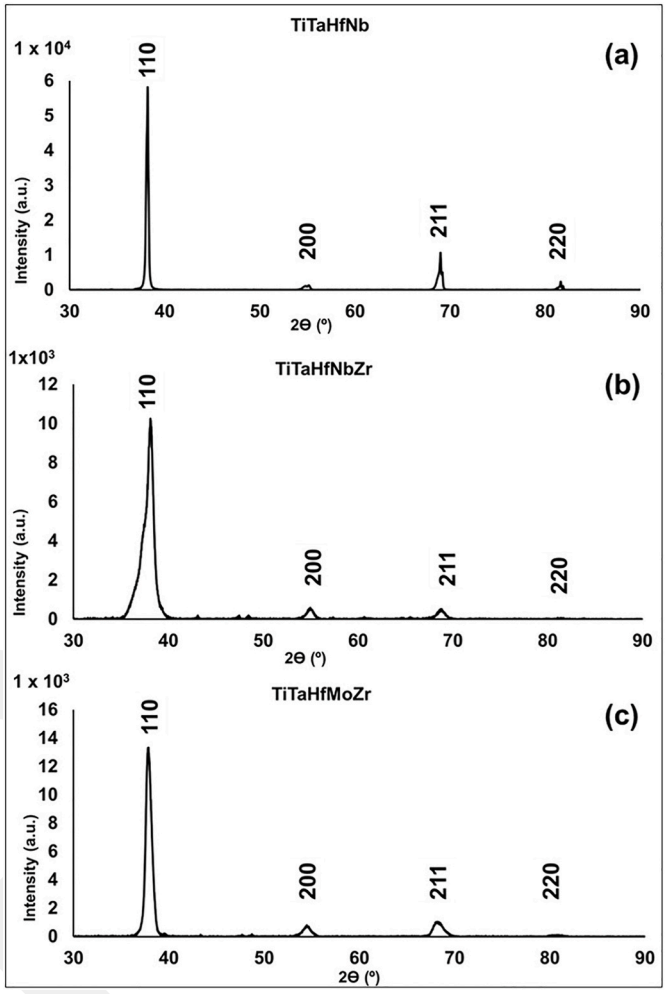

Fig. 1. XRD results of the as-received **(a)** TiTaHfNb, **(b)** TiTaHfNbZr, and **(c)** TiTaHfMoZr HEAs.

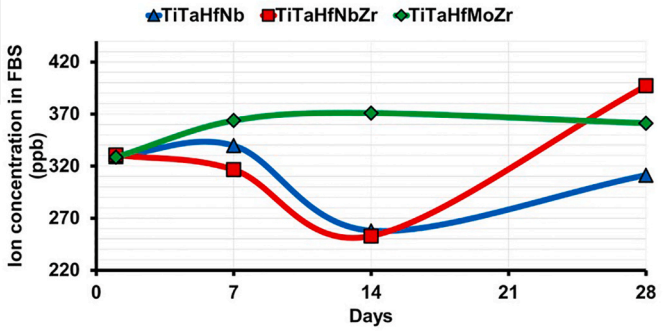

Fig. 2. Total ion concentrations in FBS following 1, 7, 14 and 28 days of immersion: total concentration of Ti, Ta and Nb ions for TiTaHfNb; total concentration of Ti, Ta, Nb and Zr ions for TiTaHfNbZr; and total concentration of Ti, Ta, Mo and Zr ions for TiTaHfMoZr. Please note that the total ion concentrations do not include Hf concentration due to its insignificant amount.

Table 2
Metal ion release from the TiTaHfNb, TiTaHfNbZr, and TiTaHfMoZr HEAs following the static immersion experiments in FBS for 28 days. Please note that the total ion concentrations do not include Hf concentration due to its insignificant amount.

	Ti (ppb)	Ta (ppb)	Nb (ppb)	Mo (ppb)	Zr (ppb)
TiTaHfNb	309.32	1.14	0.87	–	–
TiTaHfNbZr	347.24	9.34	29.86	–	10.76
TiTaHfMoZr	184.93	9.45	–	162.49	4.39

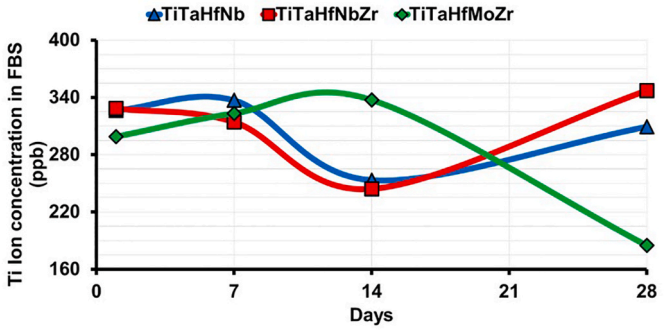

Fig. 3. Ti concentration in FBS solution upon immersion of TiTaHfNb, TiTaHfNbZr and TiTaHfMoZr samples in it for 1, 7, 14 and 28 days.

this non-homogeneous structure of the TiTaHfMoZr may lead to the significant amount of Mo release into FBS owing to the relatively lower stability of the HEA [15]. Moreover, the non-homogeneous elemental distribution during the solidification process leads to dendritic and interdendritic regions that consist of heavier and lighter elements [49], respectively, and these two distinct regions can be clearly seen in the back scattered electron (BSE) images of TiTaHfMoZr taken before the immersion tests (Fig. 5 (c) and (d)). Please note that the dentritic structures were not detected in TiTaHfNb and TiTaHfNbZr [49] by SEM and EDX as can be seen in Fig. 5 (a) and (b), and thus, only SEM images of the TiTaHfNb and TiTaHfNbZr HEAs are provided herein. The BSE image is provided for the TiTaHfMoZr HEA to show its non-homogeneous microstructure. This non-homogeneous elemental distribution did not prevail in the other two HEAs, indicating that it can be associated with the chemical bonding energy difference between Mo and Nb. However, pinpointing the exact cause remains beyond the scope of the current work and requires further elaboration.

As for the TiTaHfNb and TiTaHfNbZr HEAs, the total ion concentrations in FBS samples upon the immersion of these HEAs increase for the first 7 days, then decrease during the next seven days (14th day of immersion), and then increase concomitant with the number of days until the 28th day of the immersion tests (Fig. 2). It is important to note that the Ti ion concentration detected in the FBS samples upon immersion of these two HEAs in them follows the same trend (Figs. 2 and 3). The increase in the Ti ion concentration found in FBS samples following the first 7 days is associated with the Ti-oxide layer dissolution, mainly due to the significant amount of Ti release, while its decrease within the next seven days indicates the reformation of the oxide layer, which evidences the presence of a dissolution-reformation cycle for the TiTaHfNb and TiTaHfNbZr HEA alloys within the first 14 days [40]. Accordingly, the thickness of Ti oxide layer may decrease as the Ti concentration in FBS increases after the 14th day of immersion.

In order to further validate these arguments, surface morphologies and the corresponding elemental compositions of the TiTaHfNb, TiTaHfNbZr and TiTaHfMoZr HEAs immersed in FBS for 28 days were investigated utilizing SEM and EDX (Fig. 6). Accordingly, 25.73 at.%, 7.48 at.% and 13.69 at.% O was detected on the surfaces of TiTaHfNb, TiTaHfNbZr and TiTaHfMoZr HEAs, respectively, indicating a passive oxide layer formation on all these surfaces upon immersion in FBS. In

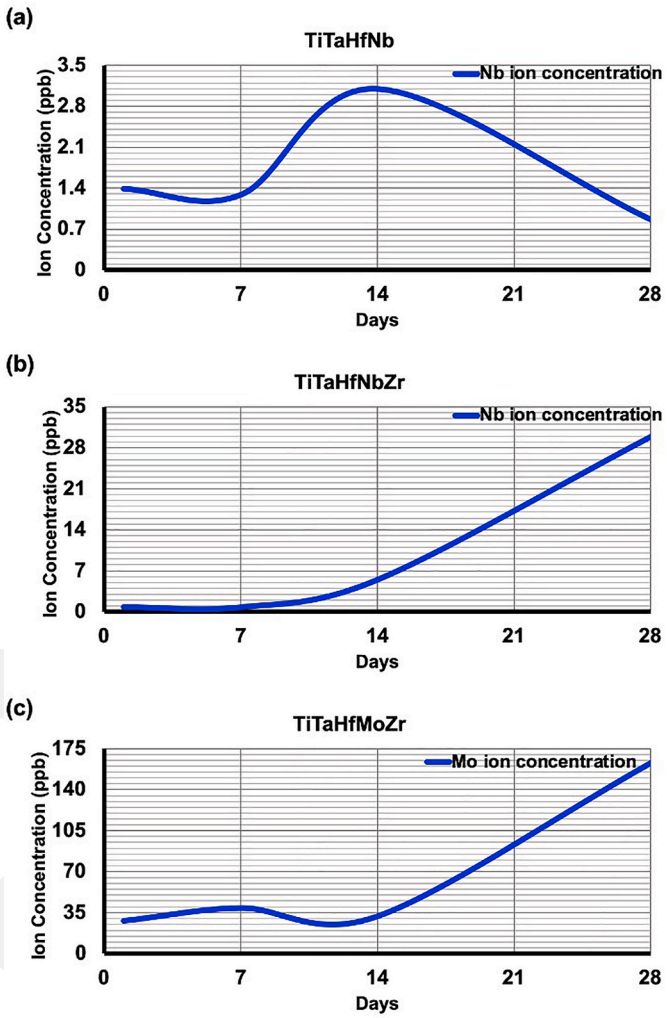

Fig. 4. (a) Concentration of Nb ions released from TiTaHfNb and **(b)** TiTaHfNbZr into FBS solution, and (c) concentration of Mo ions released from TiTaHfMoZr into FBS solution upon static immersion for 1, 7, 14 and 28 days.

order to gain further insight and detailed information regarding the passive oxide layer formation on these three HEAs upon immersion in FBS, XPS analysis was implemented to investigate the surface layer properties and elemental compositions of the samples immersed in FBS for 28 days. To begin with, the surface of the TiTaHfNb contains mainly O1s (34.3 at.% at etch time = 0), which evidences oxide layer formation following a 28-day immersion in FBS, in addition $Ca_3(PO_4)_2$ (6.1 at.%) and metal phosphate (5.7 at.%), indicating the natural formation of bone-like apatite (Fig. 7(a)), which is of utmost importance in terms of biocompatibility of an orthopedic implant material. It should be noted that Ca and P deposition on the TiTaHfNb surface facilitates hydroxyapatite formation, which enhances biocompatibility by establishing a binding between the bone and the implant material. Specifically, the layer of bone-like apatite, which is composed of $Ca_3(PO_4)_2$ and metal phosphate, was observed from the etch time of 0 s–360 s in TiTaHfNb sample that was immersed in FBS for 28 days. The bone-like apatite layer on TiTaHfNb indicates high biocompatibility of this HEA following only a 28-day immersion in FBS, and this binding layer is expected to be thicker following longer periods of contact with FBS. At etch time = 360 s, the contents of Ca and P were 1.2 at.% and 0.6 at.%, respectively, which were replaced by metals and their oxides upon further etching (Fig. 7(a)). It should be noted that the change of elemental contents were presented with respect to etch time rather than depth in Fig. 7. There are methods to calculate the depth based on etch time following ion etching,

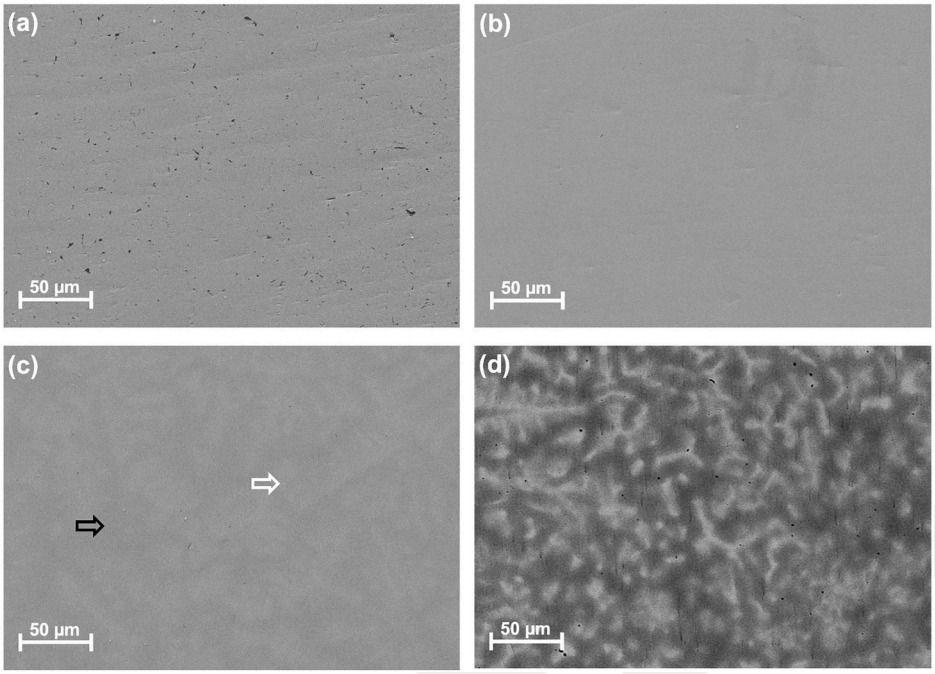

Fig. 5. SEM images of the as-received **(a)** TiTaHfNb, **(b)** TiTaHfNbZr, and **(c)** TiTaHfMoZr. The black arrow in (c) shows darker regions and the white arrow shows brighter regions that stem from the non-homogeneous elemental distribution observed in this alloy. **(d)** The BSE image of the as-received TiTaHfMoZr surface.

such as angle-resolved XPS (ARXPS) [50], however; these methods are not reliable in many cases, especially when the oxide layer is thin [51], and thus, the XPS data is presented in terms of etch time herein.

These observations are also supported by the binding energies presented in Fig. 8, such that the O1s peak is located at 530.6 eV binding energy at etch time = 0 (Fig. 8(a)), the Ca2p is located at 347.6 eV and 351.1 eV binding energies for Ca2p3 and Ca2p1, respectively (Fig. 8(b)), indicating the calcium oxidation states present in a hydroxy apatite (HA) layer on the surface of the TiTaHfNb HEA following a 28-day immersion in FBS [52–54]. In addition to the Ca peaks, the P peaks observed at 133.4 eV and 134.2 eV binding energies indicate the existence of P on the surface layer, and thereby the existence of different amorphous compounds such as $Ca(H_2PO_4)_2$ [52] (Fig. 8(c)). Finally, proteins in FBS apparently led to a high C content on the TiTaHfNb surface (etch time = 0), and C could be detected even after etching for 480 s: particularly, C1s peaks exist from the etch time = 0 s to the etch time = 480 s (Fig. 7(a)), and the corresponding C1s peaks are located at 285.5 eV and 288.2 eV binding energies of CO_2 and C. The carbon content at 288.2 eV binding energy mainly shows that C and N signals stem from proteins in the FBS [41] (Fig. 8(d)). As such, the protein adsorption facilitates biocompatibility by enhancing the binding between human tissue and the implant material.

Quite different results were obtained when Zr was added to the TiTaHfNb system to obtain the TiTaHfNbZr HEA: to begin with, the surface of the 28-day immersed samples contained O1s (17.0 at.%), P2p (0.4 at.%), and C (balance) on the surface at etch time = 0 s without metallic content (Fig. 7(b)). At etch time = 120 s, P2p disappeared, and at etch time = 240 s metals and their oxides were detected. As illustrated in Fig. 9, P peaks at 132.9 eV and 134.0 eV binding energies were observed, however; no Ca2p peaks were detected at all. Nevertheless, the deposition of P2p on the surface layer seems to have just started following 28 days of immersion in FBS, which indicates the possibility of HA formation on the TiTaHfNbZr HEA surface upon longer contact with FBS. When Nb in the TiTaHfNbZr HEA was replaced with Mo in order to obtain the TiTaHfMoZr HEA, the passive oxide layer was much thinner as compared to the other two HEAs upon immersion in FBS for 28 days. Specifically, metals appeared as early as etch time = 120 s (Fig. 7(c)), while O1s peak was detected in TiTaHfMoZr with P2p and Ca2p peaks on the surface (etch time = 0 s, Fig. 10). The interaction between Ca2p and P2p was observed until etch time = 120 s, revealing the formation of a thin HA layer on the surface, which may also be improved upon longer contact of the TiTaHfMoZr HEA with the FBS.

In addition to HA layer formation on TiTaHfNb, TiTaHfNbZr and TiTaHfMoZr HEAs, the XPS results also revealed important information regarding the Ti-oxide formation on these alloys. The XPS peaks presented in Fig. 11 show that metallic Ti was present from the etch time 360 s to etch time 1080 s in all three HEAs. In particular, for the TiTaHfNb HEA, the $Ti2p_{3/2}$ peaks at 454.1 eV and 454.0 eV binding energies for etch time 360 s and 1080 s indicate the presence of metallic Ti on the surface of TiTaHfNb for following 28 days immersion in FBS [55] (Fig. 11 (a) and (b)). Similarly, $Ti2p_{3/2}$ peaks were observed for the TiTaHfNbZr HEA at 454.1 eV and 453.9 eV and for the TiTaHfMoZr HEA at 454.0 eV and 454.9 eV binding energies for etch times 360 s and 1080 s, respectively, indicating the presence of metallic Ti on the surface following 28 days of immersion in FBS. Consequently, the XPS results support the ICP-MS results that demonstrate the initial dissolution of the Ti-oxide layer (Fig. 3), such that there is no indication of Ti-oxide layer at the etch time 360 s even though it is expected to be present close to surface. When the XPS and ICP-MS results are simultaneously evaluated, one can conclude that bone-like apatite formation (based on the existence of Ca and P peaks in XPS results) on TiTaHfNb, TiTaHfNbZr and TiTaHfMoZr HEAs following a 28-day immersion in FBS, while a fast dissolution of Ti within the first week of the immersion test are evident (Fig. 3). Overall, the HA formation on all three HEAs, and especially the TiTaHfNb HEA, indicates that these alloys possess a strong potential as orthopedic implant materials, while the evidence of reformation-dissolution cycles of the Ti-oxide layer warrants further investigations prior to drawing solid conclusions on their utility as implant materials.

As a final remark, it should be noted that the mechanical properties of the TiTaHfNb, TiTaHfNbZr and TiTaHfMoZr HEAs also contribute to their biocompatibility. Specifically, the elastic moduli of TiTaHfNb, TiTaHfNbZr and TiTaHfMoZr were measured by nano-indentation as 112.2 GPa, 131.6 GPa and 158.9 GPa, respectively. These values are lower than those of the commonly used implant materials within the 180–210 GPa range [49], indicating a better mechanical compatibility

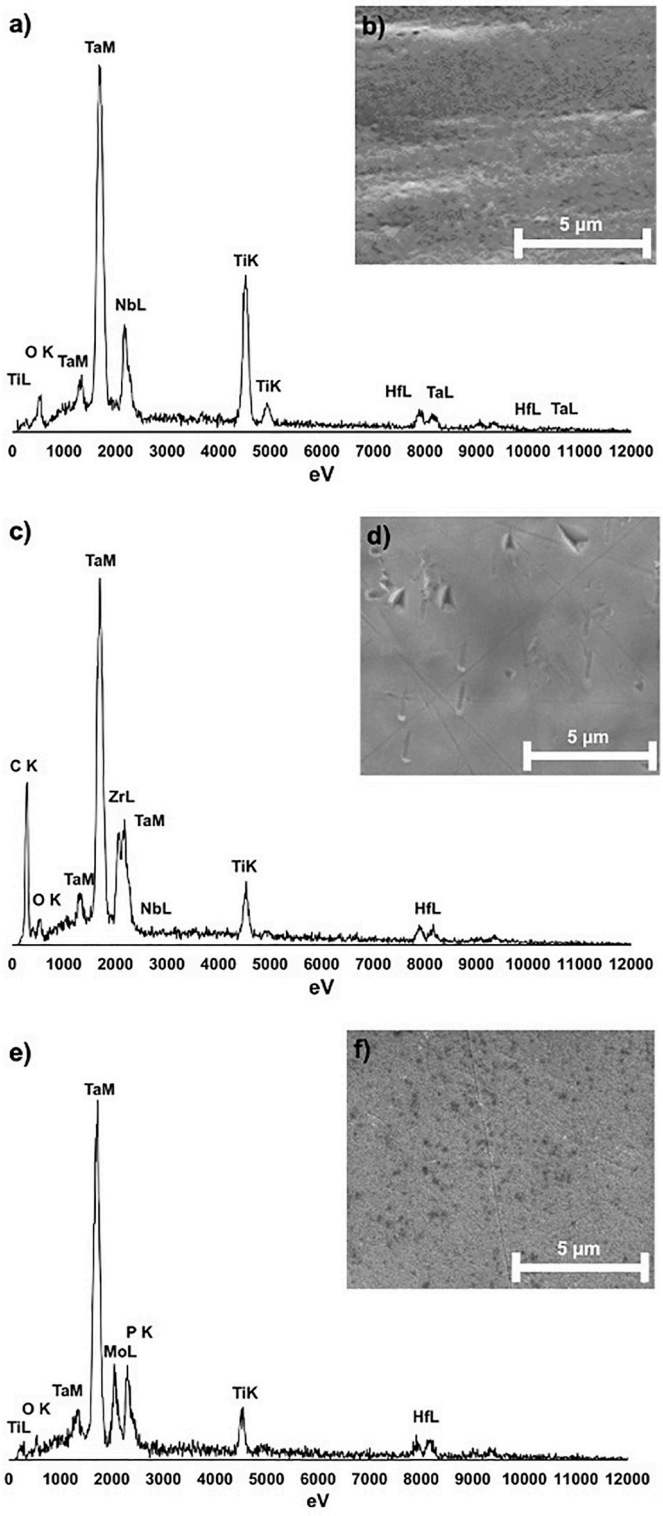

Fig. 6. EDX analysis results of the surface of **(a)** TiTaHfNb, **(c)** TiTaHfNbZr, and **(e)** TiTaHfMoZr samples immersed in FBS for 28 days: the corresponding SEM images represent the EDX scan areas of the immersed **(b)** TiTaHfNb, **(d)** TiTaHfNbZr, and **(f)** TiTaHfMoZr samples.

with the bone. Additionally, the hardness values for these three HEAs were measured as 3.5 GPa, 6.5 GPa and 6.6 GPa for TiTaHfNb, TiTaHfNbZr and TiTaHfMoZr, respectively.

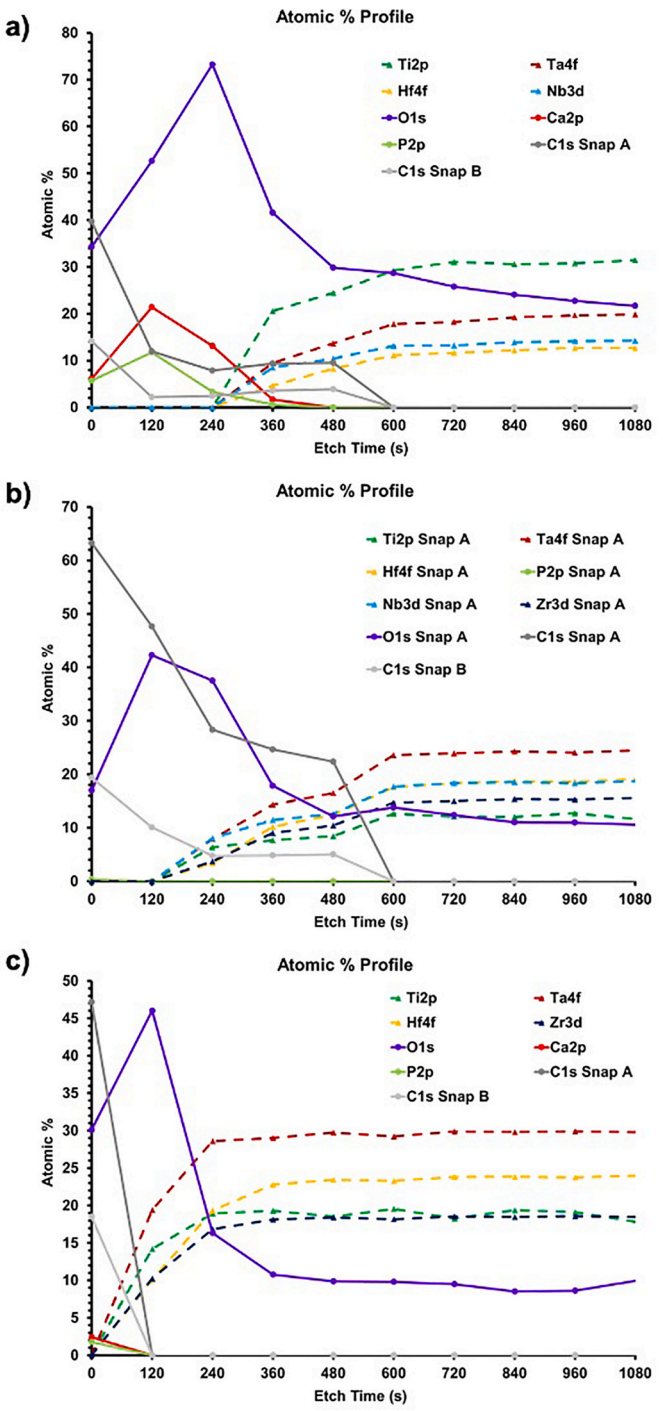

Fig. 7. Depth profiles of **(a)** TiTaHfNb, **(b)** TiTaHfNbZr, and **(c)** TiTaHfMoZr upon static immersion in FBS for 28 days.

4. Conclusions

In this work, the biocompatibility of three TiTaHf-based high entropy alloys (HEAs), namely the TiTaHfNb, TiTaHfNbZr, TiTaHfMoZr alloys, was investigated using fetal bovine serum (FBS) in order to assess the effect of proteins on the corrosion of these alloys that are considered for potential orthopedic implant applications. The experimental results presented herein indicate that the TiTaHfNb HEA exhibits the highest corrosion resistance against FBS, as evidenced by the lowest ion release from this HEA into the FBS. Moreover, bone-like apatite formation was observed following 28 days of immersion in FBS on all three HEAs

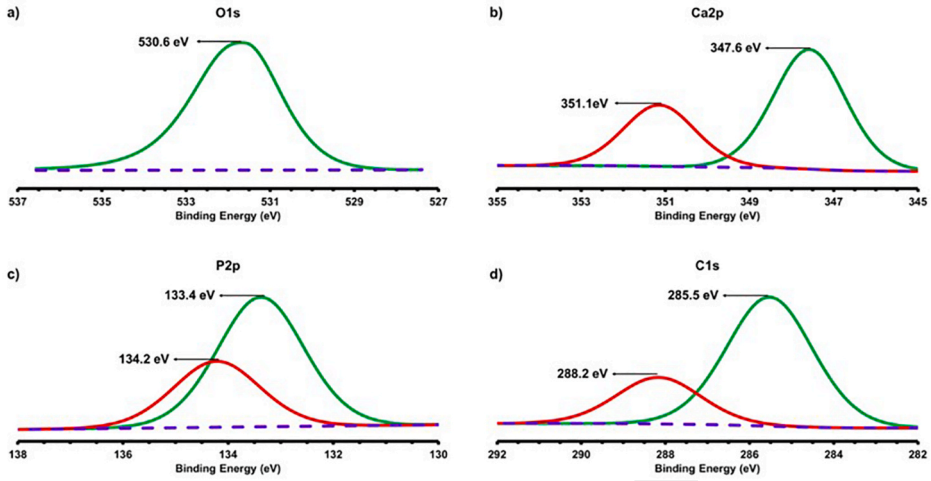

Fig. 8. XPS results of TiTaHfNb following 28 days of immersion in FBS at etch time = 0 s: **(a)** O1s peak, **(b)** Ca2p peaks, **(c)** P2p peaks, **(d)** C1s peaks.

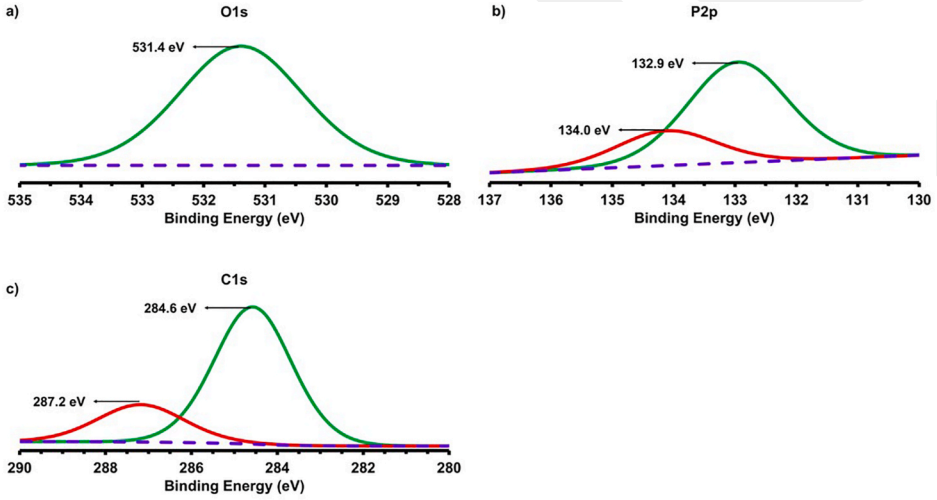

Fig. 9. XPS results of TiTaHfNbZr following 28 days of immersion in FBS at etch time = 0 s: **(a)** O1 s peak, **(b)** P2p peaks, **(c)** C1s peak.

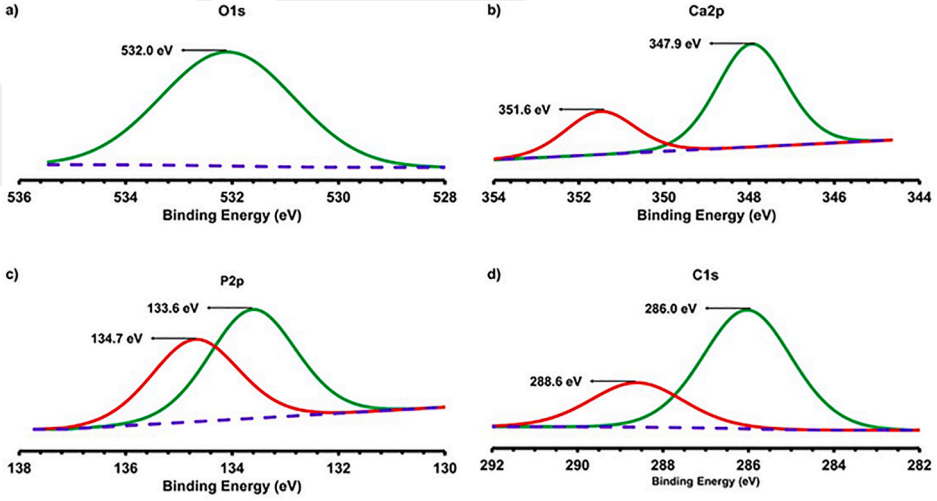

Fig. 10. XPS results of TiTaHfMoZr following 28 days of immersion in FBS at etch time = 0 s: **(a)** O1s peak, **(b)** Ca2p peaks, **(c)** P2p peaks, **(d)** C1s peaks.

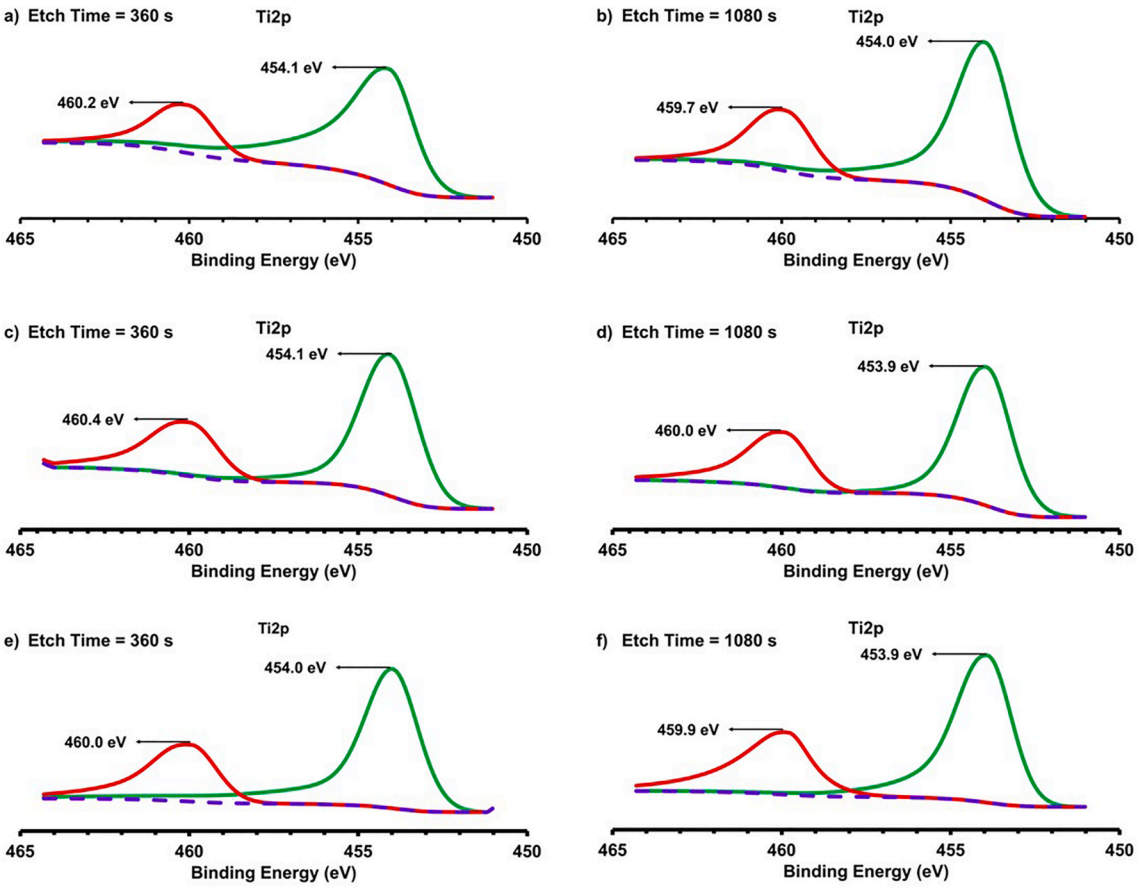

Fig. 11. Ti2p peaks following 28 days of immersion in FBS for the etch times 360 s and 1080 s: **(a)** and **(b)** for TiTaHfNb, **(c)** and **(d)** for TiTaHfNbZr, **(e)** and **(f)** for TiTaHfMoZr.

investigated in this study. More importantly, the current experimental findings indicate that the newly developed TiTaHf-based HEAs can produce hydroxy apatite on their surfaces upon coming into contact with FBS, which not only is a strong indication of their great potential for utility in orthopedic implants, but also warrants further investigation of their mechanical response and biocompatibility.

CRediT authorship contribution statement

S. Gurel: Formal analysis, Investigation, Methodology, Validation, Visualization, Writing – original draft. **A. Nazarahari:** Formal analysis, Investigation, Methodology, Validation, Visualization, Writing – original draft. **D. Canadinc:** Conceptualization, Funding acquisition, Methodology, Project administration, Resources, Supervision, Writing – original draft. **H. Cabuk:** Conceptualization, Methodology, Resources, Supervision, Writing – original draft. **B. Bal:** Funding acquisition, Resources, Writing – original draft.

Declaration of competing interest

The authors declare that they have no known competing financial interests or personal relationships that could have appeared to influence the work reported in this paper.

Acknowledgments

This work was supported by the BAGEP Award of the Science Academy. The ICP-MS analyses were conducted at Koc University Surface Science and Technology Center (KUYTAM), while the SEM, EDX and XPS analyses were carried out at Bilkent UNAM facilities. The authors are grateful to Dr. M.B. Yagci of Koc University for his help with the interpretation of the XPS results. The authors also acknowledge the financial support by the Koç University Graduate School of Sciences and Engineering. B. Bal acknowledges the AGU-BAP [grant number FAB-2017-77].

References

[1] S. Ghosh, S. Sanghavi, P. Sancheti, Metallic biomaterial for bone support and replacement, in: Fundam. Biomater. Met, Elsevier, 2018, pp. 139–165, https://doi.org/10.1016/B978-0-08-102205-4.00006-4.
[2] N. Henrik Nielsen, T. Menné, Nickel sensitization and ear piercing in an unselected Danish population, Contact Dermatitis 29 (1993) 16–21, https://doi.org/10.1111/j.1600-0536.1993.tb04530.x.
[3] B. Magnusson, M. Bergman, B. Bergman, R. Söremark, Nickel allergy and nickel-containing dental alloys, Eur. J. Oral Sci. 90 (1982) 163–167, https://doi.org/10.1111/j.1600-0722.1982.tb01540.x.
[4] M. Niinomi, Mechanical biocompatibilities of titanium alloys for biomedical applications, J. Mech. Behav. Biomed. Mater. 1 (2008) 30–42, https://doi.org/10.1016/j.jmbbm.2007.07.001.
[5] A. Biesiekierski, J. Wang, M. Abdel-Hady Gepreel, C. Wen, A new look at biomedical Ti-based shape memory alloys, Acta Biomater. 8 (2012) 1661–1669, https://doi.org/10.1016/j.actbio.2012.01.018.
[6] M. Saini, Implant biomaterials: a comprehensive review, World J. Clin. Cases. 3 (2015) 52, https://doi.org/10.12998/wjcc.v3.i1.52.
[7] P. Thomas, Assessment of immuno-allergological properties of ceramic and metallic compounds in vitro, Key Eng. Mater. 192–195 (2000) 359–362. https://doi.org/10.4028/www.scientific.net/KEM.192-195.359.
[8] M. Niinomi, Recent metallic materials for biomedical applications, Metall. Mater. Trans. 33 (2002) 477–486, https://doi.org/10.1007/s11661-002-0109-2.
[9] S. Rao, T. Ushida, T. Tateishi, Y. Okazaki, S. Asao, Effect of Ti, Al, and V ions on the relative growth rate of fibroblasts (L929) and osteoblasts (MC3T3-E1) cells, Bio Med. Mater. Eng. 6 (1996) 79–86.
[10] J.L. Domingo, Vanadium: a review of the reproductive and developmental toxicity, Reprod. Toxicol. 10 (1996) 175–182, https://doi.org/10.1016/0890-6238(96)00019-6.

[11] J.C. Wataha, G. Schmalz, Dental alloys, in: Biocompat. Dent. Mater, Springer Berlin Heidelberg, Berlin, Heidelberg, 2009, pp. 221–254, https://doi.org/10.1007/978-3-540-77782-3_8.
[12] A. Bandyopadhyay, F. Espana, V.K. Balla, S. Bose, Y. Ohgami, N.M. Davies, Influence of porosity on mechanical properties and in vivo response of Ti6Al4V implants, Acta Biomater. 6 (2010) 1640–1648, https://doi.org/10.1016/j.actbio.2009.11.011.
[13] W. Yang, Y. Liu, S. Pang, P.K. Liaw, T. Zhang, Bio-corrosion behavior and in vitro biocompatibility of equimolar TiZrHfNbTa high-entropy alloy, Intermetallics 124 (2020), 106845, https://doi.org/10.1016/j.intermet.2020.106845.
[14] M. Gueye, S. Ammar-Merah, S. Nowak, P. Decorse, A. Chevillot-Biraud, L. Perrière, J.P. Couzinie, I. Guillot, G. Dirras, Study of the stability under in vitro physiological conditions of surface silanized equimolar HfNbTaTiZr high-entropy alloy: a first step toward bio-implant applications, Surf. Coating. Technol. 385 (2020), 125374, https://doi.org/10.1016/j.surfcoat.2020.125374.
[15] S. Gurel, M.B. Yagci, B. Bal, D. Canadinc, Corrosion behavior of novel Titanium-based high entropy alloys designed for medical implants, Mater. Chem. Phys. (2020), 123377, https://doi.org/10.1016/j.matchemphys.2020.123377.
[16] A. Motallebzadeh, N.S. Peighambardoust, S. Sheikh, H. Murakami, S. Guo, D. Canadinc, Microstructural, mechanical and electrochemical characterization of TiZrTaHfNb and Ti1.5ZrTa0.5Hf0.5Nb0.5 refractory high-entropy alloys for biomedical applications, Intermetallics 113 (2019), 106572, https://doi.org/10.1016/j.intermet.2019.106572.
[17] T.D. Brown, D.L. Bartel, What design factors influence wear behavior at the bearing surfaces in total joint replacements? J. Am. Acad. Orthop. Surg. 16 (2008) S101–S106, https://doi.org/10.5435/00124635-200800001-00020.
[18] J.P. McAuley, E.S. Szuszczewicz, A. Young, C.A. Engh, Total hip arthroplasty in patients 50 Years and younger, Clin. Orthop. Relat. Res. 418 (2004) 119–125, https://doi.org/10.1097/00003086-200401000-00019.
[19] M. Synder, M. Drobniewski, M. Sibiński, Long-term results of cementless hip arthroplasty with ceramic-on-ceramic articulation, Int. Orthop. 36 (2012) 2225–2229, https://doi.org/10.1007/s00264-012-1639-x.
[20] Y.J. Hsu, W.C. Chiang, J.K. Wu, Corrosion behavior of FeCoNiCrCux high-entropy alloys in 3.5% sodium chloride solution, Mater. Chem. Phys. 92 (2005) 112–117, https://doi.org/10.1016/j.matchemphys.2005.01.001.
[21] V. Geanta, I. Voiculescu, P. Vizureanu, A. Victor Sandu, High entropy alloys for medical applications, in: High Entropy Alloy, IntechOpen, 2019, pp. 116–124, https://doi.org/10.5772/intechopen.89318.
[22] M.C. Gao, P.K. Liaw, J.W. Yeh, Y. Zhang, High-entropy alloys: fundamentals and applications. https://doi.org/10.1007/978-3-319-27013-5, 2016.
[23] M. Todai, T. Nagase, T. Hori, A. Matsugaki, A. Sekita, T. Nakano, Novel TiNbTaZrMo high-entropy alloys for metallic biomaterials, Scripta Mater. 129 (2017) 65–68, https://doi.org/10.1016/j.scriptamat.2016.10.028.
[24] Q. Ye, K. Feng, Z. Li, F. Lu, R. Li, J. Huang, Y. Wu, Microstructure and corrosion properties of CrMnFeCoNi high entropy alloy coating, Appl. Surf. Sci. 396 (2017) 1420–1426, https://doi.org/10.1016/j.apsusc.2016.11.176.
[25] S.P. Wang, J. Xu, (TiZrNbTa)-Mo high-entropy alloys: dependence of microstructure and mechanical properties on Mo concentration and modeling of solid solution strengthening, Intermetallics 95 (2018) 59–72, https://doi.org/10.1016/j.intermet.2018.01.017.
[26] Q.-T. Song, J. Xu, (TiZrNbTa)90Mo10 high-entropy alloy: electrochemical behavior and passive film characterization under exposure to Ringer's solution, Corrosion Sci. 167 (2020), 108513, https://doi.org/10.1016/J.CORSCI.2020.108513.
[27] A. Motallebzadeh, M.B. Yagci, E. Bedir, C.B. Aksoy, D. Canadinc, Mechanical properties of TiTaHfNbZr high-entropy alloy coatings deposited on NiTi shape memory alloy substrates, Metall. Mater. Trans. A Phys. Metall. Mater. Sci. 49 (2018) 1992–1997, https://doi.org/10.1007/s11661-018-4605-4.
[28] C.B. Aksoy, D. Canadinc, M.B. Yagci, Assessment of Ni ion release from TiTaHfNbZr high entropy alloy coated NiTi shape memory substrates in artificial saliva and gastric fluid, Mater. Chem. Phys. 236 (2019), 121802, https://doi.org/10.1016/j.matchemphys.2019.121802.
[29] N. Tüten, D. Canadinc, A. Motallebzadeh, B. Bal, Microstructure and tribological properties of TiTaHfNbZr high entropy alloy coatings deposited on Ti–6Al–4V substrates, Intermetallics 105 (2019) 99–106, https://doi.org/10.1016/j.intermet.2018.11.015.
[30] L. Freire, M.A. Catarino, M.I. Godinho, M.J. Ferreira, M.G.S. Ferreira, A.M. P. Simões, M.F. Montemor, Electrochemical and analytical investigation of passive films formed on stainless steels in alkaline media, Cement Concr. Compos. 34 (2012) 1075–1081, https://doi.org/10.1016/j.cemconcomp.2012.06.002.
[31] W. Rostoker, J.O. Galante, P. Lereim, Evaluation of couple/crevice corrosion by prosthetic alloys under in vivo conditions, J. Biomed. Mater. Res. 12 (1978) 823–829, https://doi.org/10.1002/jbm.820120605.
[32] G.C.F. Clark, D.F. Williams, The effects of proteins on metallic corrosion, J. Biomed. Mater. Res. 16 (1982) 125–134, https://doi.org/10.1002/jbm.820160205.
[33] A. Kocijan, I. Milošev, B. Pihlar, Ï. Ev, A. Kocijan, I. Milos, B. Pihlar, The influence of complexing agent and proteins on the corrosion of stainless steels and their metal components, J. Mater. Sci. Mater. Med. 14 (2003) 69–77, https://doi.org/10.1023/A:1021505621388.
[34] G. Gstraunthaler, T. Lindl, J. van der Valk, A plea to reduce or replace fetal bovine serum in cell culture media, Cytotechnology 65 (2013) 791–793, https://doi.org/10.1007/s10616-013-9633-8.
[35] M.G. McAlinden, D.J. Wilson, Comparison of cancellous bone-derived cell proliferation in autologous human and fetal bovine serum, Cell Transplant. 9 (2000) 445–451, https://doi.org/10.1177/096368970000900401.
[36] I. Milošev, The effect of biomolecules on the behaviour of CoCrMo alloy in various simulated physiological solutions, Electrochim. Acta 78 (2012) 259–273, https://doi.org/10.1016/J.ELECTACTA.2012.05.146.
[37] H.F. Li, X.H. Xie, K. Zhao, Y.B. Wang, Y.F. Zheng, W.H. Wang, L. Qin, In vitro and in vivo studies on biodegradable CaMgZnSrYb high-entropy bulk metallic glass, Acta Biomater. 9 (2013) 8561–8573, https://doi.org/10.1016/J.ACTBIO.2013.01.029.
[38] J.R.S. Martins Júnior, A.A. Matos, R.C. Oliveira, M.A.R. Buzalaf, I. Costa, L. A. Rocha, C.R. Grandini, Preparation and characterization of alloys of the Ti–15Mo–Nb system for biomedical applications, J. Biomed. Mater. Res. B Appl. Biomater. 106 (2018) 639–648, https://doi.org/10.1002/jbm.b.33868.
[39] J. Zhang, N. Kong, Y. Shi, J. Niu, L. Mao, H. Li, M. Xiong, G. Yuan, Influence of proteins and cells on in vitro corrosion of Mg–Nd–Zn–Zr alloy, Corrosion Sci. 85 (2014) 477–481, https://doi.org/10.1016/J.CORSCI.2014.04.020.
[40] B. Uzer, O. Birer, D. Canadinc, Investigation of the dissolution–reformation cycle of the passive oxide layer on NiTi orthodontic archwires, Shape Mem. Superelasticity. 3 (2017) 264–273, https://doi.org/10.1007/s40830-017-0114-3.
[41] R. Hang, S. Ma, V. Ji, P.K. Chu, Corrosion behavior of NiTi alloy in fetal bovine serum, Electrochim. Acta 55 (2010) 5551–5560, https://doi.org/10.1016/j.electacta.2010.04.061.
[42] V. Milleret, S. Buzzi, P. Gehrig, A. Ziogas, J. Grossmann, K. Schilcher, A. S. Zinkernagel, A. Zucker, M. Ehrbar, Protein adsorption steers blood contact activation on engineered cobalt chromium alloy oxide layers, Acta Biomater. 24 (2015) 343–351, https://doi.org/10.1016/j.actbio.2015.06.020.
[43] N.J. Hallab, J.J. Jacobs, Chemokines associated with pathologic responses to orthopedic implant debris, Front. Endocrinol. 8 (2017), https://doi.org/10.3389/fendo.2017.00005.
[44] M. Wang, Z. Ma, Z. Xu, X. Cheng, Microstructures and mechanical properties of HfNbTaTiZrW and HfNbTaTiZrMoW refractory high-entropy alloys, J. Alloys Compd. 803 (2019) 778–785, https://doi.org/10.1016/j.jallcom.2019.06.138.
[45] Y.L. Chou, J.W. Yeh, H.C. Shih, The effect of molybdenum on the corrosion behaviour of the high-entropy alloys Co1.5CrFeNi1.5Ti0.5Mox in aqueous environments, Corrosion Sci. 52 (2010) 2571–2581, https://doi.org/10.1016/j.corsci.2010.04.004.
[46] F. Lukáč, M. Dudr, J. Čížek, P. Harcuba, T. Vlasák, M. Janeček, J. Kuriplach, J. Moon, H.S. Kim, J. Zýka, J. Málek, Defects in high entropy alloy HFNBTatiZr prepared by high pressure torsion, Acta Phys. Pol., A 134 (2018) 891–894, https://doi.org/10.12693/APhysPolA.134.891.
[47] J.P. Couzinié, G. Dirras, Body-centered cubic high-entropy alloys: from processing to underlying deformation mechanisms, Mater. Char. 147 (2019) 533–544, https://doi.org/10.1016/j.matchar.2018.07.015.
[48] A. Ayyagari, R. Salloom, S. Muskeri, S. Mukherjee, Low activation high entropy alloys for next generation nuclear applications, Materialia 4 (2018) 99–103, https://doi.org/10.1016/j.mtla.2018.09.014.
[49] S. Gurel, M.B. Yagci, D. Canadinc, G. Gerstein, B. Bal, H.J. Maier, Fracture behavior of novel biomedical Ti-based high entropy alloys under impact loading, Mater. Sci. Eng. (2020), 140456, https://doi.org/10.1016/j.msea.2020.140456.
[50] R. Champarenia, P. Mack, R. White, J. Wolstenholme, Non-destructive characterization and metrology for ultra-thin high-k dielectric layers, AIP Conf. Proc. 683 (2003) 154–159, https://doi.org/10.1063/1.1622463.
[51] L. Kalina, V. Bilek Jr., M. Buso, J. Koplik, J. Masilko, Thickness determination of corrosion layers on iron using XPS depth profiling, Mater. Technol. 52 (2018) 537–540, https://doi.org/10.17222/mit.2016.180.
[52] J.P. Schreckenbach, G. Marx, F. Schlottig, M. Textor, N.D. Spencer, Characterization of anodic spark-converted titanium surfaces for biomedical applications, J. Mater. Sci. Mater. Med. (1999) 453–457, https://doi.org/10.1023/A:1008988706980.
[53] K.L. Ou, J. Wu, W.F.T. Lai, C. Bin Yang, W.C. Lo, L.H. Chiu, J. Bowley, Effects of the nanostructure and nanoporosity on bioactive nanohydroxyapatite/reconstituted collagen by electrodeposition, J. Biomed. Mater. Res. 92 (2010) 906–912, https://doi.org/10.1002/jbm.a.32454.
[54] T. Miyazaki, H.-M. Kim, T. Kokubo, C. Ohtsuki, H. Kato, T. Nakamura, Mechanism of bonelike apatite formation on bioactive tantalum metal in a simulated body fluid, Biomaterials 23 (2002) 827–832, https://doi.org/10.1016/S0142-9612(01)00188-0.
[55] M. Jenko, M. Gorenšek, M. Godec, M. Hodnik, B.Š. Batič, Č. Donik, J.T. Grant, D. Dolinar, Surface chemistry and microstructure of metallic biomaterials for hip and knee endoprostheses, Appl. Surf. Sci. 427 (2018) 584–593, https://doi.org/10.1016/j.apsusc.2017.08.007.